



Optimization of the motion of a flapping airfoil using sensitivity functions

Houssam Soueid^{a,c,1}, Laura Guglielmini^b, Christophe Airiau^c, Alessandro Bottaro^{a,*}

^a DICAT, Università di Genova, 1 Via Montallegro, 16145 Genova, Italy

^b SEAS, Harvard University, 29 Oxford Street, Cambridge, MA 02138, USA

^c IMFT, 1 Allée du Pr. Camille Soula, 31400 Toulouse, France

ARTICLE INFO

Article history:

Received 21 December 2007

Received in revised form 31 May 2008

Accepted 15 September 2008

Available online 1 November 2008

ABSTRACT

The motion of a flapping NACA0012 airfoil is optimized by means of numerical simulations for a Reynolds number equal to 1100. The control parameters are the amplitudes and the phase angles of the flapping motion in addition to the mean angle of attack. Sensitivity functions are used to compute the gradient of a cost functional related to the propulsive efficiency of the airfoil and a quasi-Newton method is adopted to drive the control parameters towards their optimal values. The ability of a flapping airfoil to produce sufficient lift and thrust forces for appropriate kinematics is demonstrated. Furthermore, a linear dependence between heaving and pitching amplitudes is found for optimal configurations leading to a constant value of the maximum effective angle of attack roughly equal to 11° . This value corresponds to the angle yielding the maximal lift-to-drag ratio for this Reynolds number when the NACA0012 airfoil does not flap. Previous results such as the high propulsive efficiency when a 90° phase angle exists between heaving and pitching, or the reversal of the von Karman street for a Strouhal number close to 0.2, are confirmed here with a new methodology. Finally, optimal kinematics for various types of missions are given and the corresponding flows are described.

© 2008 Elsevier Ltd. All rights reserved.

1. Introduction

Human craving for flight has historically been related to the observation of birds, leading in the past to postulate that flapping wings were required to fly. This assumption was widespread until Cayley bypassed it in 1799 with his concept of fixed wings airplanes equipped with a propulsive system. Thus, and for almost two centuries, flapping-wing flight was largely neglected due to the impossibility of building mobile-wing aircrafts at the human scale. However, in the last two decades, the progress in miniaturization of mechanical and electronic devices, on the one hand, and studies showing better performances of mobile wings configurations at the birds' scale [18,15] on the other, brought the attention back to flapping-wing configurations, allowing the realization of a large number of small autonomous aircrafts, usually referred to as MAVs (micro-aerial vehicles). Today, MAVs of roughly 20 cm wingspan and 10 m/s forward speed are widely used in military and civil missions including spying, surveillance, detection of chemical or biological elements, atmospheric studies and weather forecast, due to some of their features which include stealth, easy and fast deployment, low cost and real-time data acquisition [13,6].

Early attempts at designing fixed wings MAVs as small airplanes met with problems, the main one being that of finding a suitable light propulsive system (motor and batteries) able to provide the requested power during the whole duration of the mission. Despite progress in this field, the propulsive system still represents more than half the total mass of an MAV [8] allowing missions of typical duration between 30 and 60 min. A way of improving this consists in increasing the propulsive efficiency of flight, reducing the required power and optimizing the thrust. Therefore, a large number of authors studied the mechanisms used by birds and fish in order to reduce drag, delay stall, and increase maneuverability [22,26].

Lately, attention has been focused on the study of the space of relevant parameters for flapping wings, which represent the primary element of the propulsive kinematics in fish and birds, including the Strouhal number, the oscillations amplitudes and the Reynolds number [29,16,11]. The aim was to find the optimal parameters yielding good performances, like, for instance, the high propulsive efficiency (defined as the ratio of the useful to the total required power) of fish found by Lighthill [17]. In the present work, we address the optimal motion of a two-dimensional flapping airfoil by means of a sensitivity approach which directly controls the foil kinematics and minimizes a functional related to a given performance of flight. A two-dimensional approach is well known to overestimate the propulsive efficiency since it does not account properly for the trailing vorticity. However, it is still interesting to analyze the dynamics and the forces acting on the airfoil and

* Corresponding author.

E-mail addresses: houssam.soueid@unige.it (H. Soueid), alessandro.bottaro@unige.it (A. Bottaro).

URL: <http://www.dicat.unige.it/soueid> (H. Soueid).

¹ Present address: Airbus France – Site de Saint-Martin-du-Touch, EDGVT – Aircraft Performance, 316 route de Bayonne, 31060 Toulouse Cedex 9, France.

to validate a new optimization strategy. On the other hand, even three-dimensional published numerical simulations failed to appropriately quantify the effective efficiency of thrust-producing-foils as argued by Pedro et al. [20] due to overestimation of the viscous forces. Here, the small Reynolds number Re used in the numerical simulations is supposed to more than counterbalance the limitation of two-dimensionality. The conjecture is that optimal values of control parameters for small Re remain optimal when Re increases despite different values of efficiency and different aerodynamics. The thrust force, related to the distribution of pressure, is quite similar for the Reynolds numbers of this study and MAVs whereas propulsive efficiency is related to the viscous effects and hence depends directly on the value of the Reynolds number [2,23].

The originality here is the optimization approach built for an automatic identification of the optimal parameters. Starting from a given initial value of the control parameter, the optimal configuration is numerically found with a reduced computational cost with respect to sweeping the whole space of parameter. This has allowed to carry out a large number of simulations for different versions of the cost functional, with emphasis on various aerodynamic measures of performance. Furthermore, the approach adopted gives rise to a multi-parameter optimization, impossible or very long to achieve with a classical variation of the control parameter. Finally, the application of the sensitivity technique to the flapping foil problem is rather innovative.

Results show the ability of the method of carrying out an efficient optimization in a wide space of parameters. They confirm some expected conclusions such that for a Strouhal number close to 0.2 the Karman street reverses, thus leading to the production of thrust, as shown by Anderson [1], and the advantage on propulsive efficiency of considering a Strouhal number close to 0.3, a value used by a large panoply of animals [29,3]. Results also confirm the conclusion reached for a higher Reynolds number compressible flow by Isogai et al. [14] about the advantage of having pitching oscillations which lead heaving oscillations by a phase angle close to 90° . Moreover, lift production was investigated and results have shown the ability of a flapping foil to produce simultaneously sufficient lift and thrust forces for an appropriate set of control parameters. Finally, inspection of the sensitivity fields yields clues on the regions of space where flow control is more efficient, highlighting the important role played by the airfoil's tips.

2. Flapping airfoil problem

2.1. The geometry

The flapping motion is defined as a combination of translational and angular oscillations denoted heaving and pitching, respectively. Thus, a pitching center, the point around which the angular oscillations occur, is chosen and the vertical position of this point, $h(t)$, is varied in time. In this work, the airfoil pitches around a point located at one third of the chord length as shown in Fig. 1. Classically, harmonic oscillations of same frequency for heaving and pitching are considered to mimic the motion of birds' wings and fish fins. The two-dimensional airfoil considered in this work is very similar to a NACA0012 airfoil, except near the trailing edge. This airfoil is constructed by means of a Joukowski transformation, which allows to map the field external to the airfoil into the field external to a circle. A plot of the foil, zoomed in the vertical direction, is displayed in Fig. 1.

The flapping-wing problem can be solved in the laboratory fixed reference (x,y) , where x and y are, respectively, the horizontal and vertical directions. However, such a choice requires to locate the position of the foil in the grid instantaneously in order to impose the unsteady boundary conditions. This would lead to a model characterized by relatively simple equations but requiring a moving mesh algorithm [21,20,25,4]. Here, we write the governing equations in a reference frame (X,Y) which moves with the airfoil, such that X is in the direction of the airfoil's chord and Y is directly orthogonal to it (cf. Fig. 1 left). Then, the mobile reference is mapped by means of the Joukowski transformation into the plane (ξ,χ) , where a polar coordinates system (r,θ) is defined. A logarithmic transformation is used to stretch the computational grid in the radial direction and improve boundary layer resolution [5]. This approach leads to relatively complicated equations but offers the advantage of easy imposition of the boundary conditions. A plot of a coarse grid in the plane (x,y) is given in Fig. 2 to illustrate the computational domain used. The effect of the different parameters of the grid will be discussed in Section 4.2. Finally, the velocity at infinity is inclined of an angle α_0 with respect to the horizontal direction, i.e. α_0 is the mean angle of attack of the airfoil over one period of oscillation.

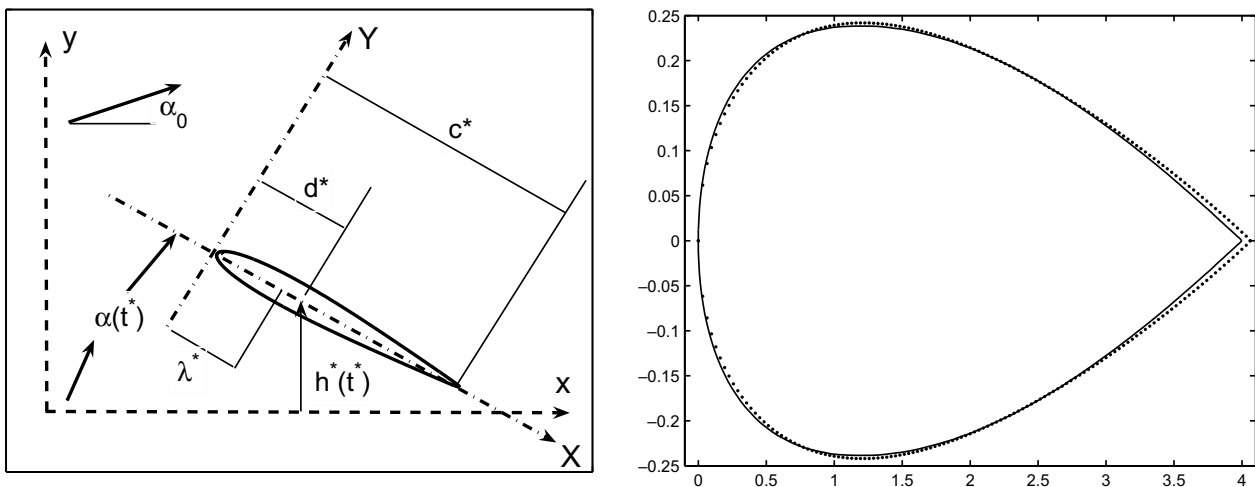


Fig. 1. Definition of the flapping motion (left) and comparison of the present airfoil (solid line) with a NACA0012 airfoil (dots) (right).

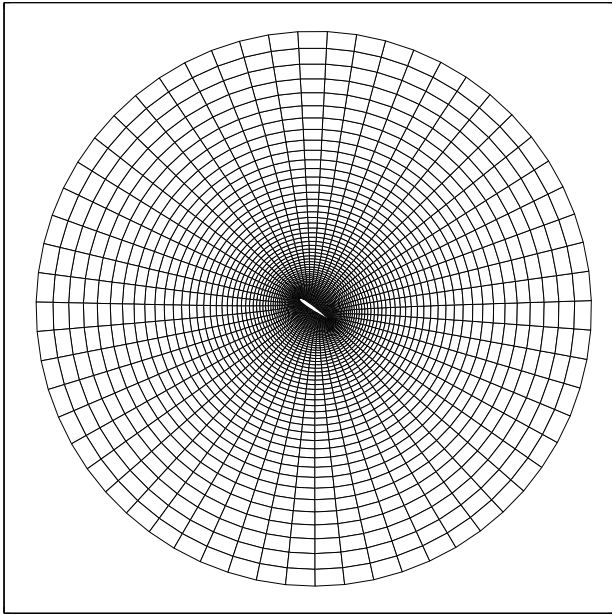


Fig. 2. Plot of a coarse grid showing the geometry of the computational domain and the effect of the logarithmic refinement near the airfoil.

2.2. The scaling

The equations of a two-dimensional incompressible flow can be reduced to two equations written in terms of the vorticity ω^* and the stream function ψ^* which are related to the velocity components (u^*, v^*) in the (x, y) reference frame by the relations:

$$\omega^* = \frac{\partial v^*}{\partial x^*} - \frac{\partial u^*}{\partial y^*}, \quad u^* = \frac{\partial \psi^*}{\partial y^*}, \quad v^* = -\frac{\partial \psi^*}{\partial x^*}$$

The superscript * denotes a dimensional quantity. For the flapping airfoil problem, two time scales can be adopted. The first is the ratio between the length scale and the velocity at infinity U_∞^* , the second is the inverse of the angular frequency of flapping σ^* measured in radians/s. The advantage of the first choice is that it allows to recover the classical Reynolds number for fixed airfoils $Re_c = \frac{U_\infty^* c^*}{\nu^*}$, where c^* is the chord length and ν^* the kinematic viscosity of the fluid. However, in a flapping foil problem this first choice prevents the study of a hovering configuration in which the velocity at infinity vanishes. Moreover, U_∞^* represents, from a physical point of view, the forward velocity of the animal and hence, depends on the flapping characteristics. Therefore, σ^* is the scaling time for the equations in the present work. Nonetheless, the classical Reynolds number may be recovered and its value will be given in the following. We consider the parameter λ^* with $\lambda^* = 0.248c^*$, as the length scale; it corresponds roughly to the position of the aerodynamic center. Some authors use the heaving amplitude as length scale but this choice cannot be adopted here since the heaving amplitude will be considered as a control parameter and hence will be variable. This is also the reason why we prefer to fix the reduced frequency f_r , rather than the Strouhal number St , defined, respectively, by $f_r = \frac{\lambda^* \sigma^*}{U_\infty^*}$ and $St = \frac{\sigma^* A^*}{2\pi U_\infty^*}$, with A^* the width of the wake usually approximated by the double of the heaving amplitude $\|h^*(t)\|$ (cf. Eq. (2)). A summary of the scales is given in Table 1.

Table 1
Reference quantities.

t^*	$v_r^*, v_\theta^*, U_\infty^*$	r^*, h^*	p^*	ω^*	ψ^*	Re	f_r	St
$\frac{1}{\sigma^*}$	$\lambda^* \sigma^*$	λ^*	$\rho^* (\lambda^* \sigma^*)^2$	σ^*	$\sigma^* \lambda^{2*}$	$\frac{\sigma^* \lambda^{2*}}{\nu^*}$	$\frac{\lambda^* \sigma^*}{U_\infty^*}$	$\frac{\sigma^* \ h^*(t)\ }{\pi U_\infty^*}$

In the table, t^* is time, v_r^* and v_θ^* the velocities in the radial and circumferential directions, p^* pressure and ρ^* the fluid density. Under these conditions, we can deduce that $Re_c = \frac{4Re}{f_r}$ and $St = \frac{\|h^*(t)\| f_r}{\pi}$, where $\|h^*(t)\| = \frac{\|h^*(t)\|}{\lambda^*}$ and $\|h^*(t)\| = \max_{t \in [0, T]} h^*(t)$. All the results which will be presented in the following, have been obtained for $f_r = 0.3665$ (for monochromatic oscillation, $St = 0.117h_1$, where h_1 is the heave amplitude when $N = 1$, cf. Eq. (2)) and $Re_c = 1100$ except in Section 7.4. The choice of such a low value of the Reynolds number allows direct numerical simulations without heavy computational costs and an easy comparison with the literature [2,21,20,11], while preserving a flow configuration with exploitable mechanisms and results. Furthermore, the secondary role played by the value of the Reynolds number has already been mentioned in Section 1 [19]. In fact, the same dependence of the thrust forces on the parameters and quantitatively comparable values of the thrust coefficients have been observed at high and low Reynolds numbers [2,23] with the counterpart of lower efficiency at low Reynolds number because of larger viscous effects. On the other hand, f_r is chosen in a way that the Strouhal number remains close to its “optimal” interval for propulsive efficiency, i.e. in the range [0.25, 0.35]. An analysis of fish swimming [29] has shown that carangiform swimmers move their tails in such a way that their Strouhal number is in this same range. In the same way, flying and running animals tune their motion to remain within this range [28,3]. A plausible value of the heaving amplitude $\|h^*(t)\|$ is often between $0.5c^*$ and c^* leading to $\|h^*(t)\|$ between 2 and 4.

2.3. The flow equations

The flow is governed by the system (1) which expresses the continuity and Navier–Stokes equations in the $(\psi - \omega)$ formulation in the polar coordinate system (r, θ) :

$$\begin{cases} \frac{\partial \omega}{\partial t} + \frac{1}{J} \left[v_r \frac{\partial \omega}{\partial r} + v_\theta \frac{\partial \omega}{\partial \theta} \right] = \frac{1}{ReJ} \left[\frac{\partial^2 \omega}{\partial r^2} + \frac{1}{r} \frac{\partial \omega}{\partial r} + \frac{1}{r^2} \frac{\partial^2 \omega}{\partial \theta^2} \right], \\ \frac{\partial^2 \psi}{\partial r^2} + \frac{1}{r} \frac{\partial \psi}{\partial r} + \frac{1}{r^2} \frac{\partial^2 \psi}{\partial \theta^2} = -J\omega, \end{cases} \quad (1)$$

where

$$\begin{aligned} v_r &= \frac{1}{\sqrt{J}} \left[\frac{\partial \psi}{\partial \theta} - \left(\dot{h}(t) \sin(\alpha(t)) - \dot{\alpha}(t) Y \right) \left(\frac{\partial X}{\partial \xi} \cos \theta + \frac{\partial X}{\partial \zeta} \sin \theta \right) \right. \\ &\quad \left. - \left(\dot{h}(t) \cos(\alpha(t)) + \dot{\alpha}(t) X \right) \left(\frac{\partial Y}{\partial \xi} \cos \theta + \frac{\partial Y}{\partial \zeta} \sin \theta \right) \right], \\ v_\theta &= \frac{1}{\sqrt{J}} \left[-\frac{\partial \psi}{\partial r} - \left(\dot{h}(t) \sin(\alpha(t)) - \dot{\alpha}(t) Y \right) \left(\frac{\partial X}{\partial \zeta} \cos \theta - \frac{\partial X}{\partial \xi} \sin \theta \right) \right. \\ &\quad \left. - \left(\dot{h}(t) \cos(\alpha(t)) + \dot{\alpha}(t) X \right) \left(\frac{\partial Y}{\partial \zeta} \cos \theta - \frac{\partial Y}{\partial \xi} \sin \theta \right) \right]. \end{aligned}$$

Dots denote derivation with respect to time t and J is the Jacobian of the Joukowski transformation which maps the coordinates of the Cartesian plane (X, Y) into the plane (ξ, ζ) . The numerical resolution of system (1) is addressed in Section 4.1.

The ω equation is solved with the value of ψ for the previous temporal step. An alternate-direction implicit (ADI) method is applied first to θ and then to r , in each case leading to a tridiagonal system solved with periodic conditions for θ and Dirichlet condition on the airfoil and Neumann condition $(\frac{\partial \omega}{\partial r} = 0)$ on the outflow boundary [10]. Once ω is computed, it is injected in the ψ Poisson-like equation solved expanding both ψ and $J\omega$ as Fourier series in the θ direction. The coefficient of these series

are determined by means of a forward fast Fourier transform algorithm. The associated boundary conditions express a vanishing velocity on the airfoil and a non-perturbed velocity at the outflow boundary. The latter condition requires a large domain to be valid and this fact increases the computational time. Finally, the system is advanced in time starting from an initial condition of zero vorticity and stream function in the whole computational domain.

2.4. The direct variables

We denote by *direct* any variable computed through the resolution of the flow equations, as opposed to sensitivity variables, which are obtained by solving the sensitivity equations. The mean values of the direct variables are obtained by averaging over T (one temporal period of oscillations in the established regime). The main direct variables are:

- The mean power required to sustain the motion of the airfoil defined as:

$$\bar{P} = -\frac{1}{T} \int_0^T [F_y(t)\dot{h}(t) + M_z(t)\dot{\alpha}(t)] dt.$$

- The mean horizontal force \bar{F} indicating whether the airfoil is dominantly producing drag ($\bar{F} > 0$) or thrust ($\bar{F} < 0$):

$$\bar{F} = \frac{1}{T} \int_0^T F_{//}(t) dt.$$

- The mean vertical force \bar{L} indicating whether the airfoil is producing lift ($\bar{L} > 0$) or not:

$$\bar{L} = \frac{1}{T} \int_0^T F_{\perp}(t) dt.$$

$F_{//}$ and F_{\perp} are, respectively, the parallel and perpendicular forces with respect to the velocity at infinity. Obviously, when $\alpha_0 = 0$, they correspond to the horizontal and vertical forces F_x and F_y in the fixed reference (x, y) . M_z is the pitching torque acting on the airfoil. We associate to these mean quantities the mean power, thrust and lift coefficients:

$$C_P = \frac{\bar{P}^*}{\frac{1}{2} \rho^* c^* U_{\infty}^{*3}} = \frac{\bar{P}}{2U_0^3}, \quad C_T = -\frac{\bar{T}^*}{\frac{1}{2} \rho^* c^* U_{\infty}^{*2}} = -\frac{\bar{F}}{2U_0^2},$$

$$C_L = \frac{\bar{L}^*}{\frac{1}{2} \rho^* c^* U_{\infty}^{*2}} = \frac{\bar{L}}{2U_0^2},$$

where $U_0 = \frac{U_{\infty}^*}{\sigma^{1/2}}$ is the non-dimensional velocity at infinity. Finally, we introduce the propulsive efficiency as the ratio of the useful power (used to fly straightforward) to the total required power:

$$\eta = -\frac{\bar{F}U_0}{\bar{P}} = \frac{C_T}{C_P}.$$

The definition of a propulsive efficiency loses interest when the airfoil is mostly producing drag ($\eta < 0$).

3. The optimization approach

3.1. Kinematics and control

The flapping motion of the airfoil is chosen by imposing an analytical expression to the heaving and pitching motions, $h(t)$ and $\alpha(t)$. In the present work, we formally generalize the classical assumption which considers a monochromatic oscillation, by writing:

$$\begin{cases} h(t) = \sum_{k=1}^N h_k \sin(kt + \tau_k), \\ \alpha(t) = \sum_{k=1}^N \alpha_k \sin(kt + \phi_k), \end{cases} \quad (2)$$

where h_k , α_k , τ_k and ϕ_k are heaving and pitching amplitudes and phases, respectively, and N is the number of modes considered. We note that, since the average over one period of $\alpha(t)$ vanishes, α_0 is the value of the angle of attack of the airfoil averaged over a period of flapping. Regardless of the value of N , the flapping motion is periodic in time with a dimensionless period equal to 2π . Thus, the numerical simulations will be carried out for a non-dimensional time multiple of 2π , representing an integer number of periods. An illustration of such a motion is given in Fig. 3 for $N = 1$, $h_1 = 4$, $\alpha_0 = 0^\circ$, $\tau_1 = 0^\circ$, $\alpha_1 = -35^\circ$ and $\phi_1 = 90^\circ$. Historically, birds' flight and fish swimming were modeled by means of simple heaving. The poor thrust developed in these conditions and its absence in hovering conditions [31,16,11] suggested the inclusion of pitching. This allows a higher thrust production via the control of leading edge vortex formation and development.

The variables h_k , α_0 , α_k , ϕ_k and τ_k for $k = 1, N$ are the parameters for which the sensitivity of the flow will be computed. Amplitudes and phases have a crucial impact on propulsion performances since they pilot the timing of the vortex shedding and propagation in the wake, whereas the average angle of attack is important for the generation of lift. The letter g will denote in the following any generic control parameter among the $4N + 1$ possible ones. The flapping airfoil configuration is known to depend on a set of 7 relevant parameters, i.e. the Strouhal number (related the flapping frequency), the heaving and pitching amplitudes, the phase between these two oscillations, the position of the pitching center, the mean angle of attack of the airfoil, and the Reynolds number based on the velocity at infinity. According to our choice of control parameters, only the position of the pitching center and the Reynolds number at infinity are constant since, in all simulations, the airfoil pitches around a point located at one third the chord length, for a Reynolds number $Re_c = 1100$ (except in Section 7.4 where frequency and Reynolds number effects are briefly considered). Guglielmini [10] has shown the positive impact of considering a pitching center in this position. This configuration is also adopted in Anderson et al. [2], where a propulsive efficiency as high as 87% is achieved. Fixing the reduced frequency and modifying the heave amplitude allow to change the Strouhal number and thus to analyze its effect.

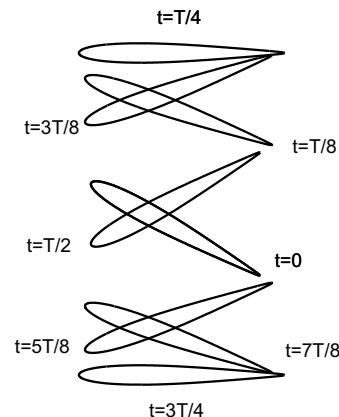


Fig. 3. Different positions of the airfoil at uniform intervals over one period for $N = 1$, $h_1 = 4$, $\tau_1 = 0^\circ$, $\alpha_0 = 0^\circ$, $\alpha_1 = -35^\circ$ and $\phi_1 = 90^\circ$.

3.2. The cost functional

The optimization process aims at improving a measure of the performances of MAVs based on flapping wings. The choice of the measure depends on the mission of the vehicle and its constraints. Hence, for a long-term mission in hostile territories, a high propulsive efficiency would be privileged, in order to increase the vehicle autonomy, whereas a mission in harsh atmospheric conditions may require high lift coefficients and/or high thrust for maneuvering. However, considering the propulsive efficiency η as the cost functional is neither indispensable nor convenient, since a peak of efficiency may be found in correspondence of insignificant thrust forces. Therefore, designers usually tune their prototypes to have a sufficient thrust with acceptable propulsive efficiency exploiting the slow decay of this latter after the peak value. Consequently, in the present work, the cost functional is written as:

$$\Upsilon = \beta^2 \bar{P} + \gamma^2 \bar{F}U_0 + \delta^2 \bar{\alpha}^2(t) + \epsilon^2 \bar{h}^2(t), \quad (3)$$

where β^2 , γ^2 , δ^2 and ϵ^2 are positive coefficients giving different weights to the different components of the cost functional, and the bar denotes time-averaging over one period of oscillation ($\bar{(\cdot)} = \frac{1}{2\pi} \int_0^{2\pi} (\cdot) dt$). The first two terms provide a balance between the required and the useful powers. A quadratic functional is not considered to properly take into account the sign of the horizontal force ($\bar{F} < 0$ when thrust is produced) avoiding optimal solutions corresponding to drag-producing kinematics. Exceptionally, for the study of the critical Strouhal number a quadratic form of the second term can be considered together with vanishing values of β^2 , δ^2 and ϵ^2 . On the other hand, a higher weight is given to thrust, with respect to power, in order to prevent the optimization process to be directed towards the trivial solution of a fixed airfoil with vanishing power and positive drag. The third and fourth terms are added to ensure a limited cost of the control and to avoid optimal solution in which the motion of the airfoil diverges. The values of δ^2 and ϵ^2 are chosen so that equivalent importance is given to the last two terms. The present functional is to be minimized leading to acceptable kinematics of the airfoil. The lift force is not included in the functional because it mainly depends on the mean angle of attack α_0 . In Section 6, lift is studied independently and an alternative cost functional is introduced.

In the configuration studied, the velocity at infinity U_0 is constant as if the optimal performance is sought for a given translational velocity of the vehicle. Therefore, U_0 does not admit variations and its presence ensures a balance between two powers. The physical configuration in which the velocity of the airfoil depends on its kinematics would be hard to simulate since it requires an analytical relationship of the type: $U_0 = U_0(\alpha_0, h(t), \alpha(t), \dots)$.

3.3. Sensitivity technique and equations

The term sensitivity denotes the derivative of a flow variable (here ω and ψ) with respect to a control parameter g . They will be referred by $\omega_{,g}$ and $\psi_{,g}$. Sensitivity functions satisfy equations which are obtained by deriving the flow Eq. (1) with respect to the control parameter(s). The solution of these equations provide a map of the hot-spots in the computational field where the flow control is most efficient. Once evaluated, sensitivities are used in the computation of the cost functional gradient. The formal expression of this gradient is:

$$\frac{d\Upsilon}{dg} = \frac{\partial \Upsilon}{\partial \omega} \frac{d\omega}{dg} + \frac{\partial \Upsilon}{\partial \psi} \frac{d\psi}{dg} + \frac{\partial \Upsilon}{\partial g}. \quad (4)$$

The last term is the partial derivative of the cost functional with respect to the control parameter whereas the first two terms are determined by isolating the parts of Υ that depend upon the flow variables and replacing ω and ψ by their sensitivities. A description of the method can be found in Gunzburger [12].

The sensitivity equations are written for a generic control parameter as:

$$\begin{cases} \frac{\partial \omega_{,g}}{\partial t} + \frac{1}{\sqrt{f}} \left[v_r \frac{\partial \omega_{,g}}{\partial r} + \frac{v_\theta}{r} \frac{\partial \omega_{,g}}{\partial \theta} + \frac{\partial v_r}{\partial g} \frac{\partial \omega}{\partial r} + \frac{1}{r} \frac{\partial v_\theta}{\partial g} \frac{\partial \omega}{\partial \theta} \right] \\ = \frac{1}{\text{Re}f} \left[\frac{\partial^2 \omega_{,g}}{\partial r^2} + \frac{1}{r} \frac{\partial \omega_{,g}}{\partial r} + \frac{1}{r^2} \frac{\partial^2 \omega_{,g}}{\partial \theta^2} \right], \\ \frac{\partial^2 \psi_{,g}}{\partial r^2} + \frac{1}{r} \frac{\partial \psi_{,g}}{\partial r} + \frac{1}{r^2} \frac{\partial^2 \psi_{,g}}{\partial \theta^2} = -J\omega_{,g}, \end{cases} \quad (5)$$

where

$$\begin{aligned} \frac{\partial v_r}{\partial g} &= \frac{1}{\sqrt{f}} \left[\frac{1}{r} \frac{\partial \psi_{,g}}{\partial \theta} - \frac{\partial}{\partial g} \left(\dot{h}(t) \sin(\alpha(t)) - \dot{\alpha}(t)Y \right) \left(\frac{\partial X}{\partial \zeta} \cos \theta + \frac{\partial X}{\partial \zeta} \sin \theta \right) \right. \\ &\quad \left. - \frac{\partial}{\partial g} \left(\dot{h}(t) \cos(\alpha(t)) + \dot{\alpha}(t)X \right) \left(\frac{\partial Y}{\partial \zeta} \cos \theta + \frac{\partial Y}{\partial \zeta} \sin \theta \right) \right], \\ \frac{\partial v_\theta}{\partial g} &= \frac{1}{\sqrt{f}} \left[-\frac{\partial \psi_{,g}}{\partial r} - \frac{\partial}{\partial g} \left(\dot{h}(t) \sin(\alpha(t)) - \dot{\alpha}(t)Y \right) \left(\frac{\partial X}{\partial \zeta} \cos \theta - \frac{\partial X}{\partial \zeta} \sin \theta \right) \right. \\ &\quad \left. - \frac{\partial}{\partial g} \left(\dot{h}(t) \cos(\alpha(t)) + \dot{\alpha}(t)X \right) \left(\frac{\partial Y}{\partial \zeta} \cos \theta - \frac{\partial Y}{\partial \zeta} \sin \theta \right) \right]. \end{aligned}$$

Compared to the flow equations, the sensitivity equations present a source term (under-braced in Eq. (5) above) which depends on the choice of the control parameter and on the flow variables. They require a prior resolution of system (1), and can be solved by the same ADI method used for the flow equations, described earlier. The associated boundary conditions are obtained through the derivation of the boundary conditions for ω and ψ with respect to g . The evolution in time occurs starting from vanishing sensitivities as initial conditions. This choice does not affect the final solution in the régime state since starting from various initial conditions has always led to the same value of the gradient. This is coherent with the fact that the value and the sign of the cost functional gradient with respect to a control parameter are independent from the means of evaluation and specifically the initial conditions.

3.4. The gradients and the optimization process

For the cases of propulsion and lift optimization, the gradients of the cost functional are, respectively:

$$\frac{d\Upsilon}{dg} = \beta^2 \frac{d\bar{P}}{dg} + \gamma^2 \frac{d\bar{F}}{dg} U_0 + \delta^2 \frac{d\bar{\alpha}^2}{dg} + \epsilon^2 \frac{d\bar{h}^2}{dg}, \quad \frac{d\Upsilon}{dg} = \frac{d\bar{L}}{dg}. \quad (6)$$

The gradient for a generic control parameter g can be expressed as:

$$\begin{aligned} 2\pi \frac{d\Upsilon}{dg} &= -\beta^2 \int_0^{2\pi} \left[\left(\frac{\partial F_x}{\partial g} + \frac{\partial F_x}{\partial \omega} \frac{d\omega}{dg} + \frac{\partial F_x}{\partial \psi} \frac{d\psi}{dg} \right) \sin(\alpha(t)) \dot{h}(t) \right] dt \\ &\quad - \beta^2 \int_0^{2\pi} \left[\left(\frac{\partial F_y}{\partial g} + \frac{\partial F_y}{\partial \omega} \frac{d\omega}{dg} + \frac{\partial F_y}{\partial \psi} \frac{d\psi}{dg} \right) \cos(\alpha(t)) \dot{h}(t) \right] dt \\ &\quad - \beta^2 \int_0^{2\pi} \left[\left(\frac{\partial M_z}{\partial g} + \frac{\partial M_z}{\partial \omega} \frac{d\omega}{dg} + \frac{\partial M_z}{\partial \psi} \frac{d\psi}{dg} \right) \dot{\alpha}(t) + M_z \frac{\partial \dot{\alpha}(t)}{\partial g} \right] dt \\ &\quad - \beta^2 \int_0^{2\pi} \left[F_x \frac{\partial(\sin(\alpha(t)))}{\partial g} \dot{h}(t) + F_x \sin(\alpha(t)) \frac{\partial \dot{h}(t)}{\partial g} \right] dt \\ &\quad - \beta^2 \int_0^{2\pi} \left[F_y \frac{\partial(\cos(\alpha(t)))}{\partial g} \dot{h}(t) + F_y \cos(\alpha(t)) \frac{\partial \dot{h}(t)}{\partial g} \right] dt \\ &\quad + \gamma^2 \int_0^{2\pi} \left[\left(\frac{\partial F_x}{\partial g} + \frac{\partial F_x}{\partial \omega} \frac{d\omega}{dg} + \frac{\partial F_x}{\partial \psi} \frac{d\psi}{dg} \right) \cos(\alpha(t) - \alpha_0) \right] dt \\ &\quad - \gamma^2 \int_0^{2\pi} \left[\left(\frac{\partial F_y}{\partial g} + \frac{\partial F_y}{\partial \omega} \frac{d\omega}{dg} + \frac{\partial F_y}{\partial \psi} \frac{d\psi}{dg} \right) \sin(\alpha(t) - \alpha_0) \right] dt \\ &\quad + \gamma^2 \int_0^{2\pi} \left[F_x \frac{\partial(\cos(\alpha(t) - \alpha_0))}{\partial g} - F_y \frac{\partial(\sin(\alpha(t) - \alpha_0))}{\partial g} \right] dt \\ &\quad + \delta^2 \frac{d\bar{\alpha}^2}{dg} + \epsilon^2 \frac{d\bar{h}^2}{dg}. \end{aligned} \quad (7)$$

Hence, the resolution of the sensitivity equations yields the values of the different derivatives which permit the estimation of the gradient. The relations which allow to compute the derivatives involved in the gradient starting from sensitivities are given in Appendix B.

Starting from a given set of values of the control parameters, the gradient of the cost functional is estimated for each parameter independently, and in succession. The control can be applied on one or more parameters at the same time, offering the opportunity to perform a multi-parameter optimization. Thus, the algorithm of optimization starts with a first iteration where a value of the parameters is imposed, $g^{(0)}$. Flow and sensitivity equations are solved for this value and the gradient with respect to g denoted $\nabla\Upsilon_g^{(0)}$ is evaluated. Two update techniques have been tested:

- The steepest descent method: $g^{(n+1)} = g^{(n)} - s\nabla\Upsilon_g^{(n)}$, where s is a relaxation parameter which must be optimized. The principle of this method is to perform a small variation of the parameter when the gradient is small i.e, when a relative optimum is being reached. An example of the application of this method to flapping foil optimization with an optimal step can be found in [30].
- The quasi-Newton algorithm: $g^{(n+1)} = g^{(n)} - \frac{g^{(n)} - g^{(n-1)}}{\nabla\Upsilon_g^{(n)} - \nabla\Upsilon_g^{(n-1)}} \nabla\Upsilon_g^{(n)}$. In this case, a first order finite difference approximation of the second derivative is used to enrich the search of the optimal direction of update.

The negative signs in the expressions above ensure that a minimum of the functional is being pursued. The quasi-Newton method is very efficient, whereas the steepest descent method requires sub-iterations for the determination of the optimal step. Alternatively, it is possible to use a small constant step, albeit with considerable increase of the number of iterations.

4. Numerical aspects

4.1. Discretization schemes

The governing equations are discretized with a second-order scheme in space. A centered scheme is applied in the core of the computational domain, whereas second order upwind and backward schemes are used near the airfoil and the outflow boundaries, respectively, for computing first and second-order derivatives.

Time advancement is accomplished with a first order upwind scheme applied in the two sub-steps of the ADI method. Time averaging is done with a trapezoidal integration on the last (useful) temporal period of the simulations.

4.2. Adequacy of grid and time step

Before initiating the parametric study, it is important to verify the independence of the results upon the grid. The numerical discretization depends on five parameters:

- R_{max} , the size of the circular computational domain, which results from a compromise between the computational cost and a proper application of the boundary conditions at the outflow boundary;
- N_r , the number of points in the radial direction;
- N_θ , the number of points in the circumferential direction;
- R_{int} , an internal radius related to the logarithmic refinement, with half the points in the radial direction located between the airfoil and this radius. The choice of this parameter for a fixed number of points is a compromise between a good resolution of the boundary layer and a good resolution of the far wake;
- N_T , the number of temporal steps in a period of oscillations, with $\Delta t = \frac{2\pi}{N_T}$.

We have computed for several different grids the error in percentage with respect to a very refined grid, for direct variables and for gradients. Results have shown that the grid defined by ($R_{max} = 45, R_{int} = 12, N_\theta = 512, N_r = 500, N_T = 10,000$) gives the best computational cost-to-accuracy ratio. Hence, this grid has been adopted in the following. The temporal step was further decreased in some configurations with large heaving amplitudes where large patches of vorticity are shed, or when the pitching angle is close to zero, a configuration characterized by a thin boundary layer.

An example of simulation is provided in Fig. 4, which shows that the initial transient lasts about one period of time.

4.3. Optimization update

To illustrate the difference between the steepest descent and the quasi-Newton methods, we minimize with respect to h_1 a cost functional defined as:

$$\Upsilon = \bar{P} + \bar{F} + \bar{\alpha}^2(t) + \bar{h}^2(t).$$

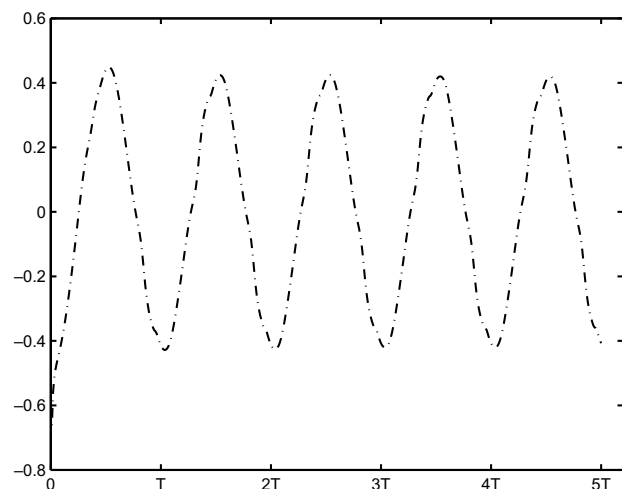
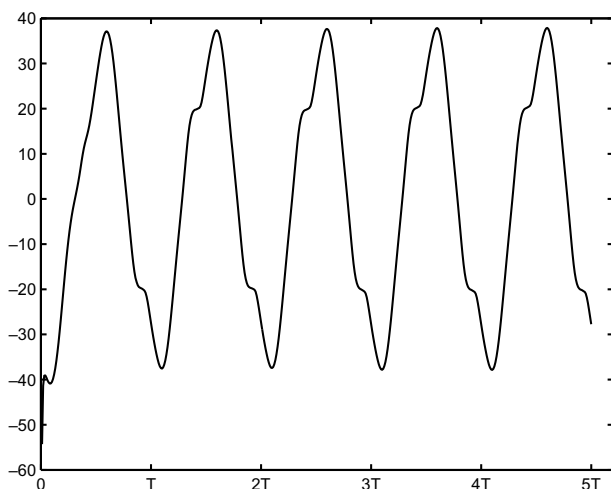


Fig. 4. Evolution of a direct variable (lift force) (left) and its sensitivity with respect to h_1 (right).

We consider the case $N = 1, h_1^{(0)} = 4.25, \alpha_0 = \tau_1 = 0, \alpha_1 = -25^\circ, \phi_1 = 90^\circ$. For the steepest descent method, the update algorithm employs a relaxation step $s = 0.01$, whereas for the quasi-Newton method we use:

$$\begin{cases} g^{(1)} = g^{(0)} - 0.25 \text{sign}(\nabla \Upsilon_g^{(0)}), \\ g^{(n+1)} = g^{(n)} - \frac{g^{(n)} - g^{(n-1)}}{\nabla \Upsilon_g^{(n)} - \nabla \Upsilon_g^{(n-1)}} \nabla g^{(n)}, \quad \text{for } n \geq 1. \end{cases}$$

The same minimum for $h_1 = 0.748$ ($St = 0.087$) is reached after 8 iterations with the quasi-Newton methods versus 37 iterations for the steepest descent method (Fig. 5). This discrepancy in performance could be reduced through a better choice of the update step s , but the speed of the quasi-Newton method is such that it has been the method of choice for all further calculations.

4.4. Validation

The flow solver has been previously validated [11] by comparison to similar numerical and experimental configurations

[7,2,31]. The validation of the sensitivity equations can be done by verifying the condition of vanishing gradient at the minimum of the cost functional. On the other hand, the resolution of the flow equations allows to recover the direct variables (\bar{P}, \bar{F}) for different values of the control parameter. Then, a “theoretical” gradient can be computed by a simple second order finite differences scheme and compared to the gradient computed with Eq. (7). Such a gradient is, however, poorly suited for a multi-parameter configurations. Besides, its accuracy is related to the control parameter step size, and hence, is generally less accurate than the computed gradient. Therefore, the cost functional in Eq. (3) with the weights $(\beta^2, \gamma^2, \delta^2, \epsilon^2) = (1, 2, 1, 1)$ is considered and control is carried out with respect to the heaving amplitude in one modal harmonic oscillation with $\alpha_1 = -25^\circ$ and $\phi_1 = 90^\circ$.

The agreement between the minimum of the cost functional and the vanishing of the gradient, and between the “theoretical” and real gradients, are very satisfactory when controlling the heaving amplitude, as shown in Fig. 6. Similar results are obtained when other control parameters are considered.

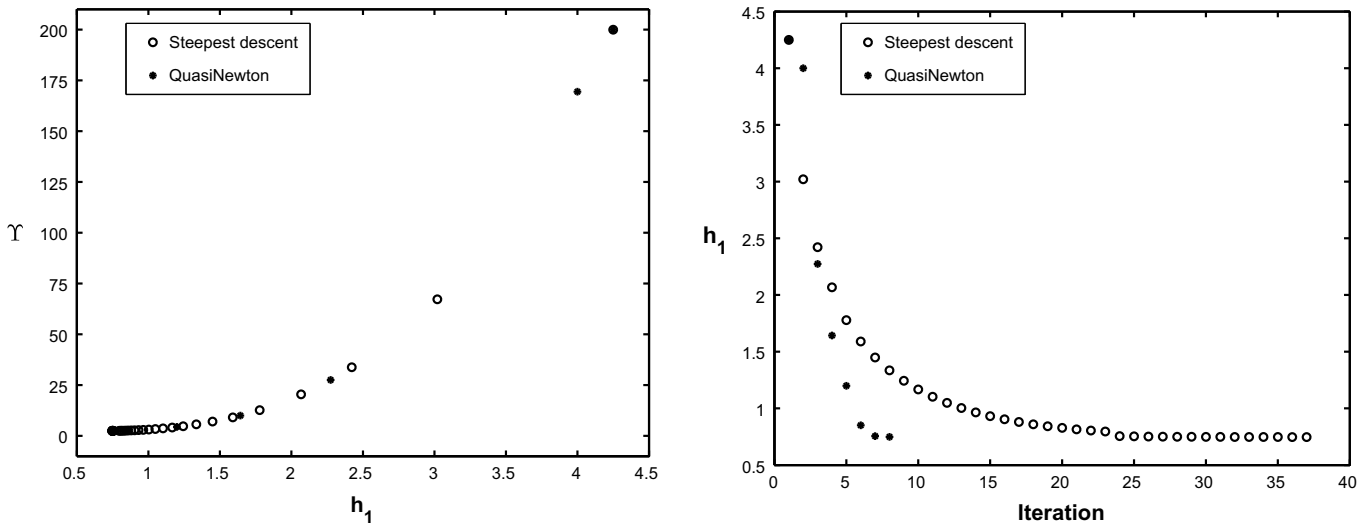


Fig. 5. Comparison of the update methods by showing the values of the cost functional (left) and the values of the control parameter (right) in the course of the iterations.

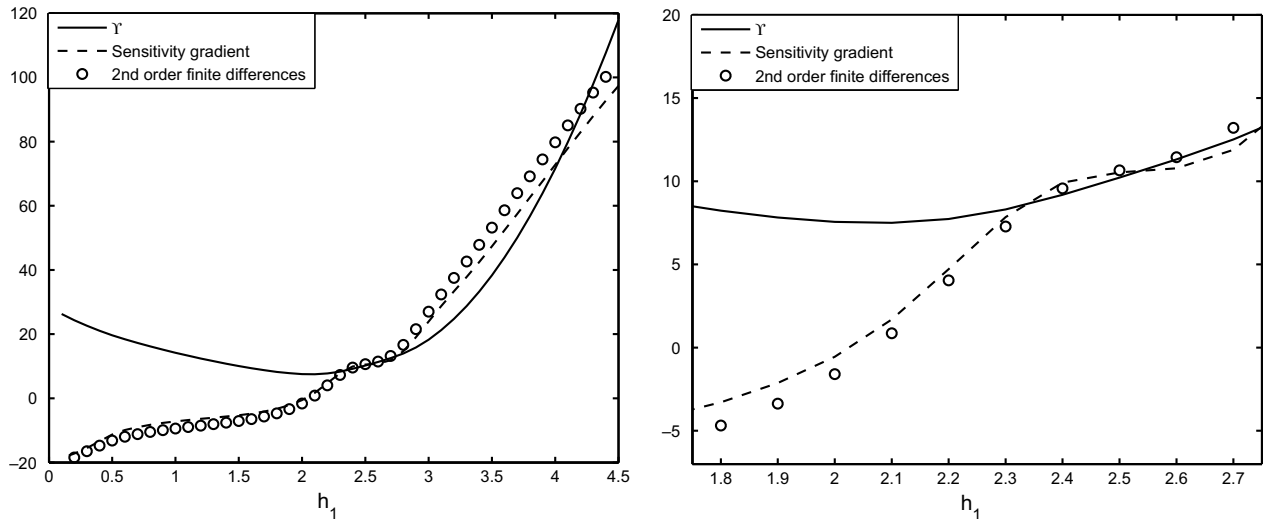


Fig. 6. Validation of the gradient computation. Left: the cost functional, in Eq. (3), right: zoom of the cost functional near its minimum. Solid lines denote the functional, dashed lines its gradient computed with sensitivity method in comparison to the second order finite-difference method (circles).

4.5. Sensitivity fields

Exploring the fields $\omega_{,g}$ and $\psi_{,g}$ allows to identify the most sensitive areas where controlling vorticity and stream function has the major effect. Sensitivity fields of the vorticity with respect to various control parameters have roughly the same topology: an expected vanishing sensitivity where vorticity vanishes and a high sensitivity near the airfoil and in the wake. The main difference when controlling different parameters lies in the numerical values of the sensitivities. Looking at the color scale in Figs. 7 and 8, we note that the pitching angle sensitivity field is characterized by higher values than the sensitivity field with respect to the phase angle, which is, itself, larger than the sensitivity with respect to the heaving amplitude. However, the regions of large sensitivity have roughly the same location for the two fields. As for vorticity, the maximal and minimal values of the sensitivity with respect to the control parameters are located near the tips of the airfoil (leading and trailing edges) confirming the crucial role of the airfoil's tips in the generation and shedding of vorticity. Similar conclu-

sions can be drawn when looking at a different instant during the oscillation.

5. Propulsion optimization

5.1. Critical Strouhal number

Before studying the effect of each control parameter on the cost functional, the critical value of the Strouhal number for different pitching angles is sought. This critical value indicates the threshold for which the reversed von Karman street occurs, leading to thrust production. For a two-dimensional airfoil which oscillates exactly at this critical value, a neutral wake, defined as an alternation of clockwise and counterclockwise rotating aligned vortices, is observed. The weights are set to $\beta^2 = \delta^2 = \epsilon^2 = 0$ and the gradient, with respect to the heaving amplitude h_1 , of the quadratic function \bar{F}^2 , is $2 \bar{F} \nabla \bar{F}$.

For the reduced frequency used here, results in Fig. 9 indicate that for a purely pitching airfoil, thrust production requires a

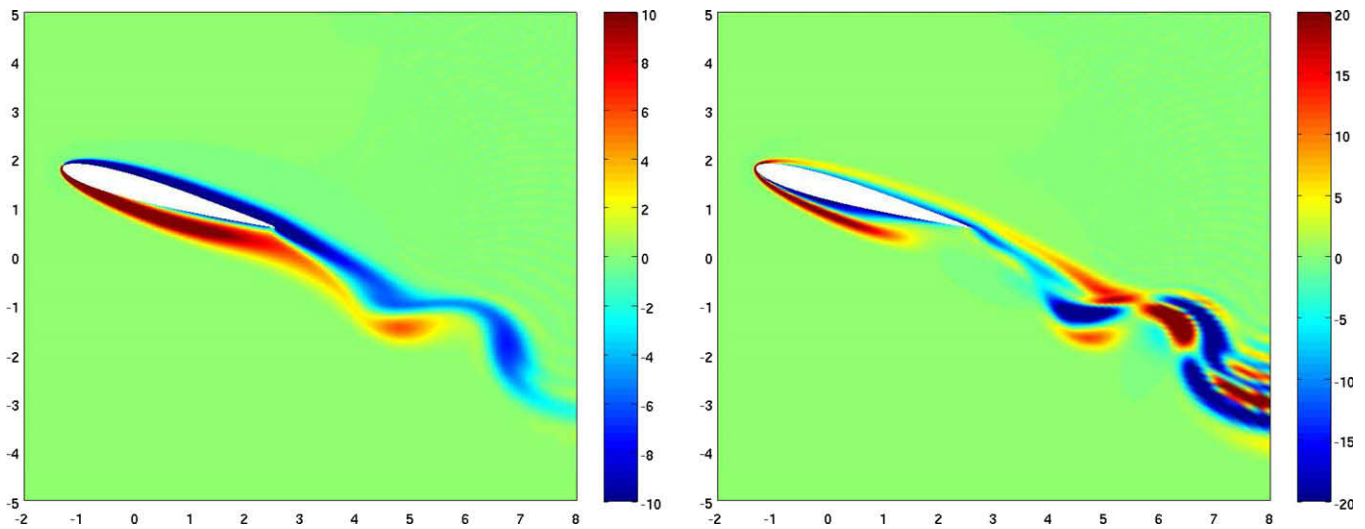


Fig. 7. Zoom near the airfoil of the vorticity field (left) and its sensitivity with respect to the heaving amplitude h_1 (right) for $N = 1$, $h_1 = 2$, $\alpha_0 = \tau_0 = 0^\circ$, $\alpha_1 = -25^\circ$ and $\phi_1 = 90^\circ$ at $t = \frac{9T}{8}$.

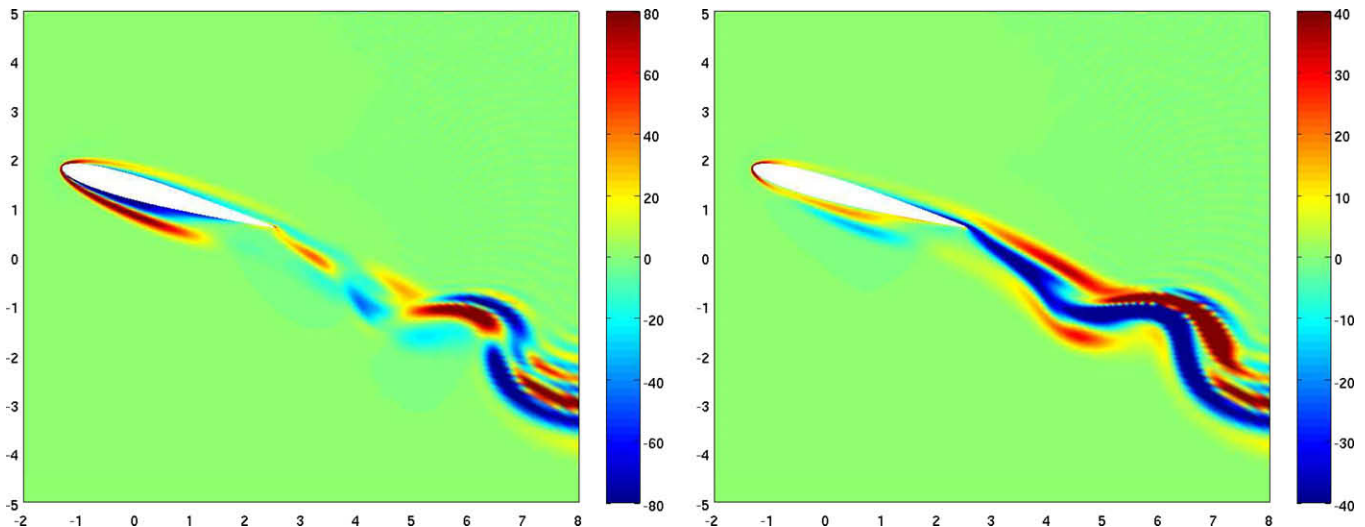


Fig. 8. Sensitivity fields of the vorticity with respect to the pitching amplitude α_1 (left) and with respect to the phase angle ϕ_1 (right) for $N = 1$, $h_1 = 2$, $\alpha_0 = \tau_0 = 0^\circ$, $\alpha_1 = -25^\circ$ and $\phi_1 = 0^\circ$ at $t = \frac{9T}{8}$.

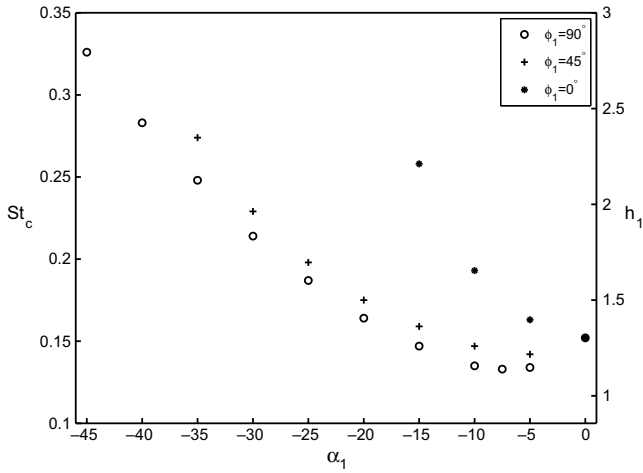


Fig. 9. Evolution of the critical Strouhal number for different pitching angle amplitudes for $N = 1$, $\tau_1 = \alpha_0 = 0^\circ$ and $\phi_1 = 0^\circ$ (filled circles), $\phi_1 = 45^\circ$ (pluses) and $\phi_1 = 90^\circ$ (empty circles).

Strouhal number greater than 0.152, value close to that found experimentally by Anderson [1] (roughly 0.2). For a flapping airfoil, thrust production is less constraining in terms of Strouhal number for small pitching angles, since a minimal critical Strouhal number of 0.133 is observed for a pitching angle close to -7.5° when a 90° phase difference between heaving and pitching is considered. Large values of the pitching angle require larger heaving amplitudes and hence a higher Strouhal number at constant frequency in order to reverse the von Karman street. The critical values increase when the phase ϕ_1 decreases from 90° towards 0° . The interest of considering a phase close to 90° has been highlighted by Streitlien et al. [27] and Isogai et al. [14]; this configuration supports the reduction of flow separation and increases flight efficiency by piloting the timing of vortex shedding from airfoil tips so that leading edge vortices interact constructively with the trailing edge vortex leading to two vortices deposited per flap [2,16].

In conclusion, for acceptable pitching angles no thrust production can be observed for $h_1 < 1$ which corresponds to an airfoil with a heaving amplitude smaller than a quarter of its chord. If a vanishing phase angle has to be studied, a pitching amplitude in the interval $[-20^\circ, 0^\circ]$ must be considered. Beyond this range, no thrust production has been observed. In the same way, and for $\phi_1 = 45^\circ$, there is no possible thrust production for $\alpha_1 < -35^\circ$. In the remainder of this work, we will focus on control parameters within favorable ranges for thrust production.

5.2. Effect of heaving and pitching amplitudes

We start by controlling the first mode of oscillation focusing, respectively, on the effect of the heaving and pitching amplitudes. First, for different values of the pitching amplitude, the minimum of the propulsive-related cost functional is sought, then, the method is inverted and for some plausible values of the heaving amplitude, the optimal value of the pitching amplitude is found. The computations are done for a configuration with a constant phase ϕ_1 equal to 90° . The results in Fig. 10 show a linear dependence between the optimal heaving amplitudes and the optimal pitching angles. We note that for a vanishing pitching angle, the optimal solution is a vanishing heaving amplitude corresponding to a still airfoil. However, with the selected cost functional this trivial solution is not the global optimal solution since lower values of the cost functional can be reached for different pitching amplitudes as shown Fig. 11.

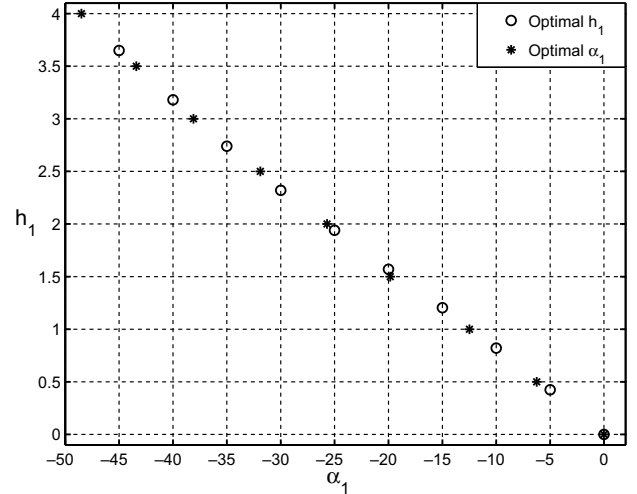


Fig. 10. Optimal (h_1, α_1) couples for $N = 1$, $\tau_1 = 0^\circ$, $\alpha_0 = 0^\circ$ and $\phi_1 = 90^\circ$. Empty circles are obtained by controlling the heaving amplitude for various pitching amplitudes whereas filled circles correspond to controlling the pitching amplitude for various heaving amplitudes.

For heaving amplitude control, the optimal solutions for $\alpha_1 > -20^\circ$ correspond to dominantly drag-producing configurations. The global minimum is obtained for $h_1 = 2.321$ and $\alpha_1 = -30^\circ$ which gives rise to $C_T = 0.229$ and $\eta = 0.398$. Higher efficiencies and/or thrust forces are achieved for $\alpha_1 < -30^\circ$ since for $\alpha_1 = -45^\circ$, we have an optimal heaving amplitude $h_1 = 3.651$ yielding $C_T = 0.601$ and $\eta = 0.466$. The latter result highlights the importance of the choice of the cost functional; it is important, however, to keep in mind that in the present section only one parameter is controlled. Furthermore, large amplitude heaving oscillations are not desirable because of the structural constraints related to such a configuration. This result illustrates the significance of including the last term (the cost of the control) in the global cost functional.

For pitching amplitude control, the global optimal solution can be found for $h_1 = 2.5$ and $\alpha_1 = -31.91^\circ$ confirming the advantage of being close to this range of control parameters. The associated performances are $C_T = 0.28$ and $\eta = 0.423$. Better values can be found for higher heaving amplitudes (for example, for $h_1 = 4$ and $\alpha_1 = -45.34^\circ$ we have $C_T = 0.90$ and $\eta = 0.485$) but, as mentioned before, such solutions do not account for the cost of performing the control. The optimal solutions obtained for $h_1 < 1.5$ correspond to dominantly drag-producing flapping airfoil.

The effect of both heaving and pitching amplitudes can be studied when considering the real angle of attack seen by the airfoil defined as:

$$\Gamma^*(t^*) = \alpha_0 + \arctan\left(\frac{\dot{h}^*(t^*)}{U_\infty^*}\right) + \alpha(t^*)$$

or, in non-dimensional form:

$$\Gamma(t) = \alpha_0 + \arctan\left(\frac{\dot{h}(t)}{U_0}\right) + \alpha(t),$$

which is the effective angle between the axis of the airfoil in motion and the direction of velocity at infinity.

The maximum value of this angle plays a crucial role for the propulsive efficiency [1,23]. For $N = 1$ and for harmonic heaving and pitching oscillations, we can write that $\Gamma_{max} \leq \alpha_0 + \arctan(\frac{h_1}{U_0}) + \alpha_1$. The main observation to be made here is that for all optimal couples (h_1, α_1) corresponding to mainly thrust-producing configurations, the maximum angle of attack is roughly constant in the interval $[10^\circ, 12.25^\circ]$ (cf. Fig. 12). This range of

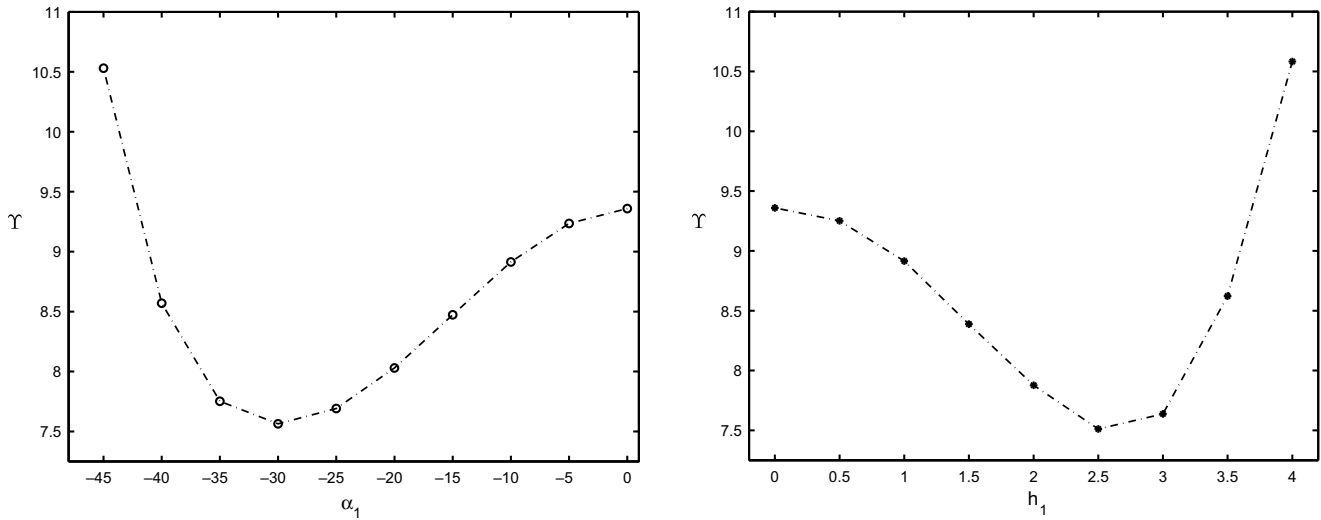


Fig. 11. Evolution of the propulsion-related cost functional at optimal values of h_1 for various α_1 (left) and at optimal values of α_1 for various h_1 (right) for $N = 1$, $\tau_1 = \alpha_0 = 0^\circ$ and $\phi_1 = 90^\circ$.

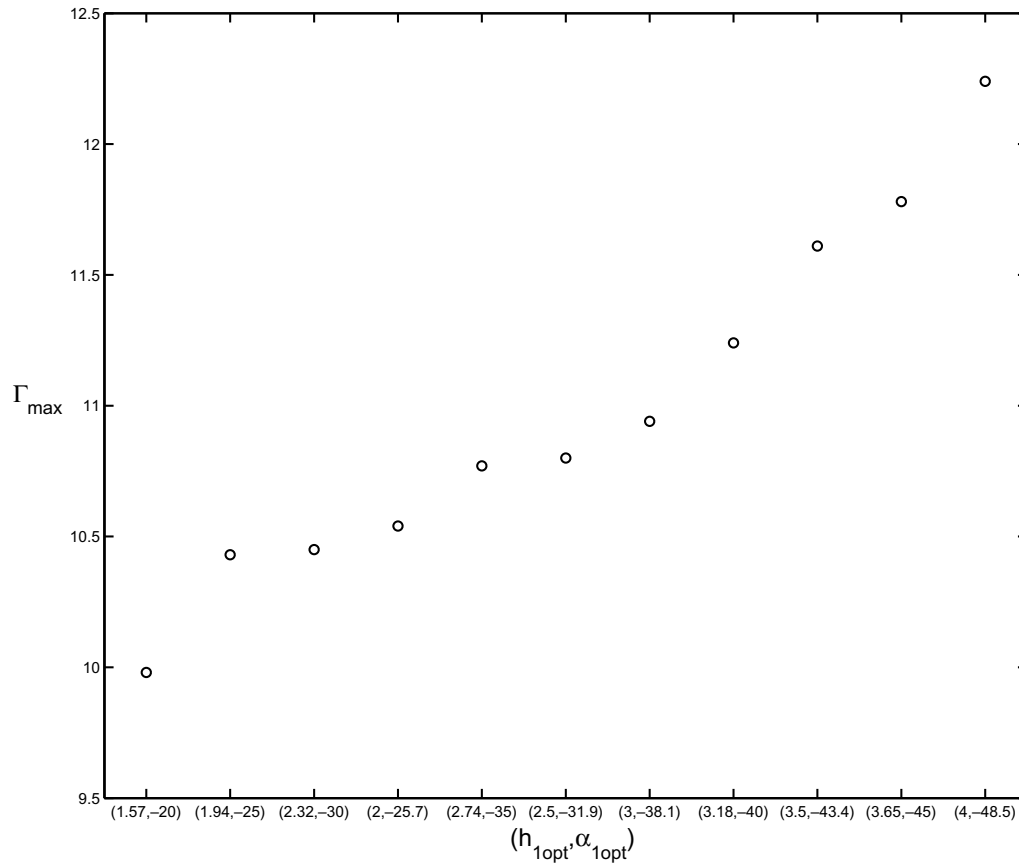


Fig. 12. Maximum values of the effective angle of attack $\Gamma(t)$ for the optimal couples of heaving and pitching amplitudes $(h_{1opt}, \alpha_{1opt})$ for $N = 1$, $\tau_1 = \alpha_0 = 0^\circ$ and $\phi_1 = 90^\circ$.

angles of attack corresponds to a good lift-to-drag ratio range for a fixed NACA0012 airfoil and within the stall angle for the Reynolds number considered here (cf. Section 6).

5.3. Effect of the phase angles ϕ_1 and τ_1

Here, the effect of the relative phase angle ϕ_1 between heaving and pitching oscillations is analyzed. Hence, for different pitching

amplitudes α_1 , the optimal ϕ_1 is computed for $h_1 = 2$ and $h_1 = 3$. The evolution is not linear, but the main conclusion is that for any plausible pitching and heaving amplitudes, the optimal phase remains roughly in the interval $[70^\circ, 90^\circ]$. This result can be related to the difficulty of generating thrust for small values of ϕ (Section 5.1) without considering very large oscillations.

Previous contributions [27,14] highlighted the advantage of considering a flapping motion in which pitching oscillations lead

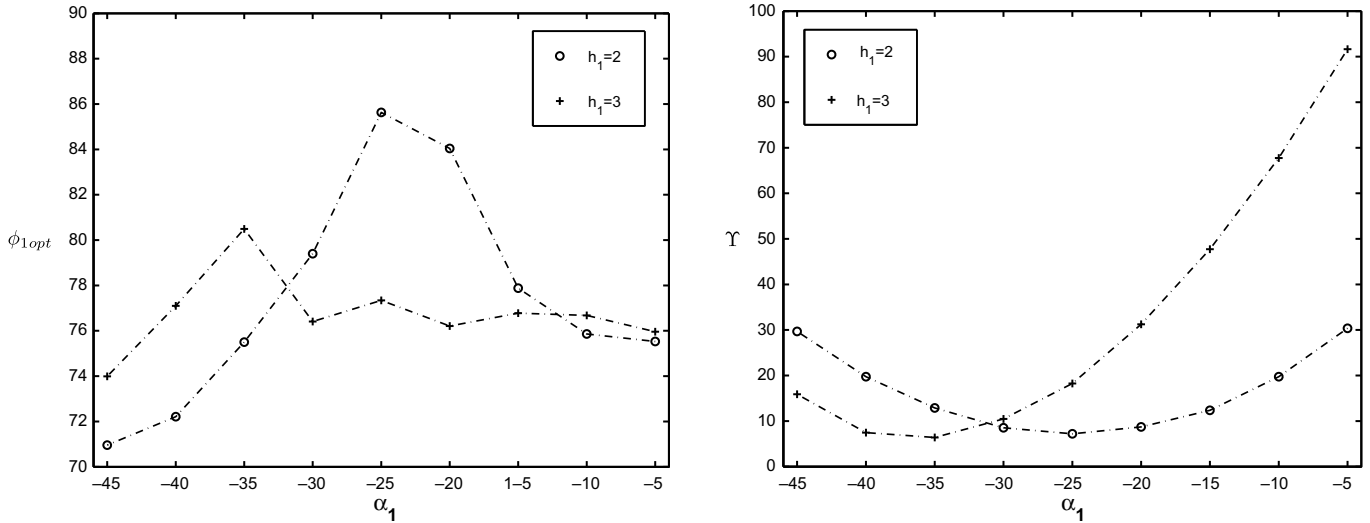


Fig. 13. Optimal phase angle ϕ_1 for various pitching amplitudes α_1 for $N = 1$, $\tau_1 = \alpha_0 = 0^\circ$ and $h_1 = 2$ and $h_1 = 3$ (left) and the corresponding values of the propulsion-related cost functional Υ (right).

heaving oscillations by an angle in the interval $[80^\circ, 100^\circ]$. It can be shown that for such a phase, leading edge vortices interact constructively with the trailing edge vortex enhancing thrust production and improving efficiency. This result, already presented in the works of Anderson et al. [2] and Lewin and Haj-Hariri [16], is obtained here by means of sensitivity optimization. Obviously, no optimal phase angle is sought for a vanishing pitching amplitude. The minimum of the cost functional for the values considered is obtained for $h_1 = 3$, $\alpha_1 = -35^\circ$ and $\phi_1 = 80.5^\circ$ leading to $C_T = 0.526$ and $\eta = 0.481$.

On the other hand, for $N = 1$, one angle ϕ_1 or τ_1 is enough to describe the phase between heaving and pitching. Therefore, the values of optimal τ_1 for $\alpha_1 \in [-45^\circ, 0^\circ]$ and $h_1 = 2$ or $h_1 = 3$ can be deduced from optimal values of ϕ_1 present in Fig. 13. The demonstration relies on a simple change of variables since we can move from:

$$\begin{aligned} h(t) &= h_1 \sin(t) & \text{to} & & h(t) &= h_1 \sin(t + \tau_1) \\ \alpha(t) &= \alpha_1 \sin(t + \phi_1) & & & \alpha(t) &= \alpha_1 \sin(t) \end{aligned}$$

by introducing $t' = t + \phi_1$, which implies that $\tau_{1opt} = -\phi_{1opt}$.

6. Lift optimization

In the present section, attention shifts on the lift produced by flapping airfoils. The results previously described (cf. Section 5) were obtained for a vanishing value of the mean angle of attack α_0 , so that both the foil motion and the flow field turn out to be symmetric with respect to the x -axis. Consequently, the mean lift force averaged over one period of oscillations vanishes: during the up-stroke a high pressure zone is observed on the upper side of the airfoil and inversely a low pressure zone is created on the bottom surface leading to a negative lift force. The mechanism is inverted during the down-stroke and an equivalent positive lift force is generated compensating the latter one. An illustration of this sequence of positive and negative values is given in Fig. 4 (left).

Lift optimization is carried out considering \bar{L} or (equivalently C_L) as the cost function and the angle α_0 as the only control parameter with the other parameters maintained constant. The case of a flapping airfoil is very different from the case of the classical fixed airfoil where lift increases proportionally to the angle of attack before reaching stall. Here, due to pitching oscillation, flow

separation occurs at different instants of the flapping motion so that the classical notion of stall cannot be invoked.

A first important conclusion is related to the presence of lift increase after the first downshoot (“stall”) (cf. Fig. 14), behavior which is recovered for different combinations of heaving and pitching amplitudes. Furthermore, if the mean angle of attack is further increased, the lift coefficient tends to saturate to an asymptotic value slightly smaller than the second peak value for certain values of h_1 and α_1 . This asymptotic behavior was also observed by Silin et al. [24] who varied the angle of attack of a flexible flapping wing between 0° and 90° . In that work, it was not possible to clearly identify stall, since the lift coefficient, after having reached a peak value, slightly decreased and then reached a roughly constant value upon increase of the angle of attack.

The second main result is the possibility to reach lift coefficients of the order of $C_L = 3$ with a flapping airfoil by a judicious choice of the angle of attack. We point out that for flapping MAVs flying at low speeds and facing gust or harsh conditions, having a large lift coefficient is indispensable for remaining airborne and maneuvering. However, and unfortunately, the maximum of lift usually corresponds to a dominantly drag-producing configuration. Therefore, it is preferable to tune the kinematics to ensure sufficient lift while thrust still can be produced maintaining angles of attack roughly $<20^\circ$.

The high values of C_L and the absence of pronounced stall seem to depend more on the low value of the Reynolds number than on the motion of the airfoil. That is the reason why we plot the lift coefficient for the same NACA0012 airfoil when it is fixed and for the same Reynolds number for various values of the mean angle of attack α_0 . For comparison, we compute the lift coefficient for the same airfoil and for the same number of Reynolds using Fluent² and Overture³ in the laminar unsteady viscous configuration. Overture has been also applied for flapping airfoil configurations and yielded very good agreement with the present results in terms of magnitude of the forces and wake topology [9].

The angle of attack for maximum lift is equal to 45° which is very large compared to the stall angle of NACA airfoils for typical flight Reynolds number of order 10^6 . However, and as soon as α_0 exceeds 20° the drag force becomes so important and the flow so

² <http://www.fluent.com>

³ <http://www.llnl.gov/casc/Overture/>

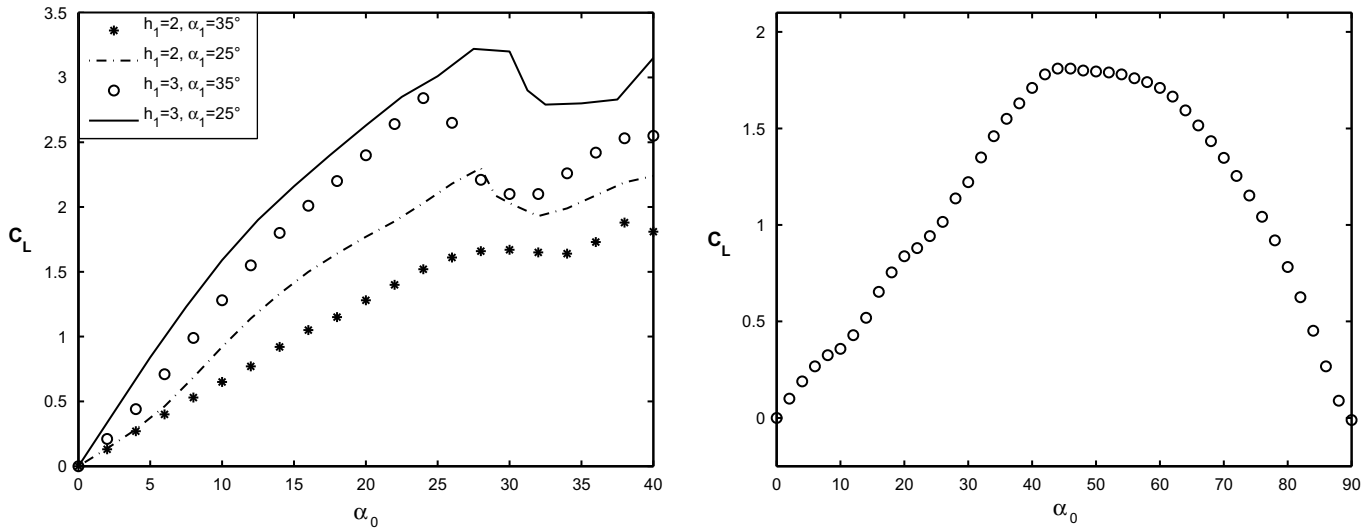


Fig. 14. Evolution of the lift coefficient with the mean angle of attack α_0 for a flapping airfoil (left) for $N = 1$, $\tau_1 = 0^\circ$, $\phi_1 = 90^\circ$ and $(2, -35^\circ)$ (filled circles), $(2, -25^\circ)$ (dot dashed line), $(3, -35^\circ)$ (empty circles) and $(3, -25^\circ)$ (solid line) and for a still airfoil (right).

unsteady that it may prevent the use of such large angles of attack. Actually, the maximum lift-to-drag ratio is equal to 2.43 and it is obtained for $\alpha_0 = 11^\circ$. This result is interesting since it was found that the optimal (h_1, α_1) yielded an effective maximal angle of attack Γ_{max} in the range $[10^\circ, 12^\circ]$.

Finally, we highlight the fact that if we fix all the control parameters except α_0 , which we increase starting from 0° , the propulsive efficiency η decreases until the airfoil starts to dominantly produce drag. This justifies the choice to accomplish the control in the previous section (Section 5) for a vanishing angle of attack.

7. Multi-parameter optimization

After having optimized separately each one of the control parameters, we seek now the optimal combination of the parameters for a given measure of performance of the airfoil. Therefore, we consider three different cases. The first two cases correspond to non-lifting airfoils, such as the fin of fish, whereas the third case corresponds to a bird or MAV configuration. The choice of considering cases where α_0 vanishes is motivated by the fact that for all combinations of amplitudes and phases (h_1, α_1, ϕ_1) and τ_1 , the cost functional is larger when α_0 is not equal to zero. In other words, if we control the five parameters at the same time, the optimal solution will be for $\alpha_0 = 0$. Therefore, we fix $\alpha_0 = 0$ in the first two cases and we control the other parameters, then, we fix α_0 to a positive value ensuring a sufficient lift and we control the amplitudes and phases for this value of the mean angle of attack.

7.1. The “basic” solution

In this case, we seek a configuration in which the airfoil produces thrust with acceptable efficiency and without very large oscillations to limit structural dynamics constraints. Hence, we minimize the following cost functional:

$$\Upsilon = \bar{P} + 2\bar{F}U_0 + 15.14\bar{\alpha}^2(t) + \bar{h}^2(t),$$

where δ^2 , the weight for $\bar{\alpha}^2$, is chosen in a way to give equivalent importance to the two terms related to cost of the control. In this case, α_0 and τ_1 are not controlled and chosen equal to zero. The optimal triplet reached here is $(h_1, \alpha_1, \phi_1) = (2.82, -32.15^\circ, 85.45^\circ)$ leading to $C_T = 0.512$, $\Gamma_{max} = 15.47^\circ$ and $\eta = 0.502$.

7.2. The “thrust” solution

Here, we seek a solution where the airfoil produces a large thrust force with acceptable efficiency without worrying about the cost of control. Thus, we minimize the following cost functional:

$$\Upsilon = (C_T - 2)^2.$$

The optimal triplet reached in this case is $(h_1, \alpha_1, \phi_1) = (4.512, -33.45^\circ, 89.68^\circ)$ leading to $C_T = 2$, $\Gamma_{max} = 26.27^\circ$ and $\eta = 0.381$.

7.3. The “practical” solution

Finally, we consider the “practical” case of requiring that the airfoil produces both lift and thrust with acceptable propulsive efficiency. Therefore, we fix $\alpha_0 = 8^\circ$. This value is chosen because it gives rise to sufficient lift force (cf. Section 6) without a large recirculation region. Then, we minimize:

$$\Upsilon = \bar{P} + 2\bar{F}U_0 + 15.14\bar{\alpha}^2(t) + \bar{h}^2(t).$$

The optimal solution is $(h_1, \alpha_1, \phi_1) = (3.85, -44.15^\circ, 86.52^\circ)$, corresponding to $C_T = 0.892$, $\Gamma_{max} = 23.94^\circ$ and $\eta = 0.417$.

A summary of all optimal results is given in Table 2 for $N = 1$, $\tau_1 = 0^\circ$, $Re_c = 1100$ and $f_r = 0.3665$.

The plot of vorticity fields for the basic solution, on the one hand, and for the low efficiency configuration, on the other, showed that high efficiency is related to a flow which remains attached to the airfoil for the whole period of oscillations, i.e. to the absence of large separation bubbles.

7.4. A note frequency and Reynolds number effect

The values of thrust coefficient and, especially, efficiency are quite low for optimal values. As the Reynolds number Re_c is increased between 1100 and 4000, an increase of roughly 7% of the efficiency is observed (cf. Fig. 15). On the other hand, the increase of the reduced frequency maintaining constant the heaving amplitude has the effect of enhancing the Strouhal number, thus further increasing the thrust coefficient. This is confirmed by the high Strouhal number needed in the “thrust” solution.

Table 2
Summary of optimal configurations.

Case	α_0 (°)	h_1	α_1 (°)	ϕ_1 (°)	St	Γ_{\max} (°)	η	C_T	C_L	C_P
h_1 control	0	2.321	−30	90	0.271	10.45	0.398	0.229	0	0.575
α_1 control	0	2.500	−31.91	90	0.29	10.80	0.423	0.280	0	0.662
ϕ_1 control	0	3.000	−35	80.50	0.35	17.55	0.481	0.526	0	1.06
Basic	0	2.820	−32.15	85.45	0.33	15.47	0.502	0.512	0	1.02
Thrust	0	4.512	−33.45	89.68	0.53	26.27	0.381	2	0	5.25
Practical	8	3.85	−44.15	86.52	0.45	23.94	0.417	0.892	0.888	2.14

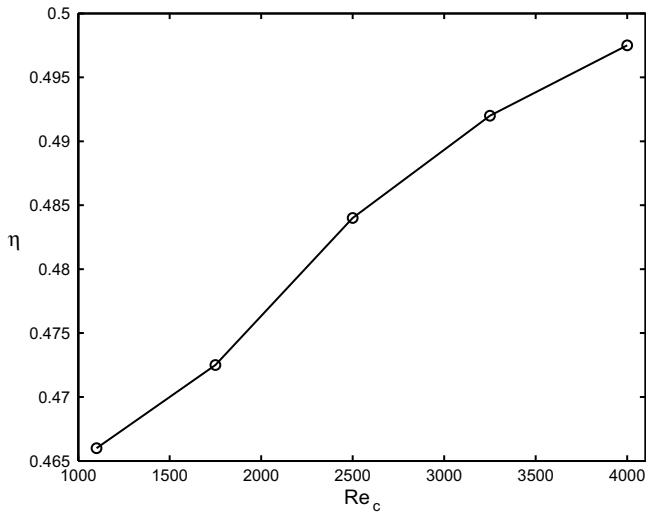


Fig. 15. Evolution of propulsive efficiency η with the Reynolds number Re_c for $N = 1$, $\alpha_0 = 0^\circ$, $h_1 = 3$, $\tau_1 = 0^\circ$, $\alpha_1 = -35^\circ$, $\phi_1 = 90^\circ$ and $f_r = 0.3665$.

8. Conclusions and perspectives

The optimization of the kinematics of a flapping airfoil is carried out controlling the airfoil’s motion parameters. The approach used is numerical and two-dimensional for a low Reynolds number configuration. Sensitivity functions are applied and allow to compute the gradient of a functional related to the propulsive efficiency with respect to the control. A quasi-Newton update method is employed to drive the parameters towards their optimal values. The present study shows that a flapping airfoil requires a smaller Strouhal number than a heaving airfoil in order to reverse the von Karman street (St is of order 0.13). The heaving and pitching amplitudes have been optimized independently showing a linear relation between optimal h_1 and optimal α_1 , and yielding a constant maximum effective angle of attack in the range $[10^\circ, 12^\circ]$. This range is close to the maximum lift-to-drag ratio angle at the same value of the Reynolds number when the airfoil does not flap. The optimization of the phase angle between heaving and pitching confirms the interest of having pitching oscillations leading by an angle close to 90° . Finally, many parameters were controlled simultaneously in order to reach a combination allowing good efficiency, with large thrust and lift forces. The optimal efficiency found here is roughly equal to 50% which might seem at first sight as a low value; however, it is not so low after consideration is given of the viscous forces at play in this configuration. Increasing the Reynolds number results in better efficiency, and high efficiency is linked to attached flow for the whole period of the oscillations.

The next step of this work is to carry out an in-depth investigation of the Strouhal number, controlling both the physical frequency and the wake width, and to perform higher Reynolds number simulations. Furthermore, the tools are now in place to handle the general case $N > 1$, and to confirm the preliminary observations by Read et al. [23] that the presence of higher

harmonics might yield larger thrust coefficients without loss in efficiency.

Acknowledgments

We acknowledge Prof. Paolo Blondeaux for several useful discussions, and Mr. Joel Guerrero for carrying out some validation runs using an independent, Chimera-based, numerical approach.

Appendix A. The flow equations

The dependence of the direct variables upon the control parameters can be written explicitly when expressing these variables in the airfoil-related reference frame (X, Y) . We write the direct variables as follows:

– Mean power:

$$\bar{P} = -\frac{1}{T} \times \int_0^T [F_X(t) \sin(\alpha(t)) \dot{h}(t) + F_Y(t) \cos(\alpha(t)) \dot{h}(t) + M_Z(t) \dot{\alpha}(t)] dt,$$

– Mean horizontal force:

$$\bar{F} = \frac{1}{T} \int_0^T [F_X(t) \cos(\alpha(t) - \alpha_0) - F_Y(t) \sin(\alpha(t) - \alpha_0)] dt,$$

– Mean vertical force:

$$\bar{L} = \frac{1}{T} \int_0^T [F_X(t) \sin(\alpha(t) - \alpha_0) + F_Y(t) \cos(\alpha(t) - \alpha_0)] dt,$$

where F_X , F_Y and M_Z are, respectively, the horizontal and vertical forces in the airfoil related frame (X, Y) and the torque acting on the airfoil. These quantities depend on the pressure and velocity gradients at the foil surface through the relations:

$$\begin{cases} F_X &= \int_0^{2\pi} (-p \frac{\partial Y}{\partial \theta} + \frac{2}{Re} [\frac{\partial Y}{\partial \theta} \frac{\partial U}{\partial X} - \frac{1}{2} \frac{\partial X}{\partial \theta} (\frac{\partial U}{\partial Y} + \frac{\partial V}{\partial X})]) d\theta, \\ F_Y &= \int_0^{2\pi} (p \frac{\partial X}{\partial \theta} + \frac{2}{Re} [\frac{1}{2} \frac{\partial Y}{\partial \theta} (\frac{\partial U}{\partial Y} + \frac{\partial V}{\partial X}) - \frac{\partial X}{\partial \theta} \frac{\partial V}{\partial Y}]) d\theta, \\ M_Z &= \int_0^{2\pi} p (X \frac{\partial X}{\partial \theta} + Y \frac{\partial Y}{\partial \theta}) d\theta \\ &+ \int_0^{2\pi} \frac{2}{Re} [-X \frac{\partial X}{\partial \theta} \frac{\partial V}{\partial Y} + \frac{1}{2} (X \frac{\partial Y}{\partial \theta} + Y \frac{\partial X}{\partial \theta}) (\frac{\partial U}{\partial Y} + \frac{\partial V}{\partial X}) - Y \frac{\partial Y}{\partial \theta} \frac{\partial U}{\partial X}] d\theta, \end{cases}$$

where U and V are the velocity components in the X and Y directions. The resolution of the flow equations (1) allows to determine the vorticity and stream function fields and consequently the velocity and pressure fields. The pressure is recovered from the equation:

$$p(\theta) = p_0 + \int_0^\theta (\frac{\partial p}{\partial X} \frac{\partial X}{\partial \theta} + \frac{\partial p}{\partial Y} \frac{\partial Y}{\partial \theta}) d\theta,$$

where p_0 is a reference pressure and

$$\begin{cases} \frac{\partial p}{\partial X} &= [\ddot{\alpha}(t)Y + \dot{\alpha}^2(t)X - \ddot{h}(t) \sin(\alpha(t))] + \frac{1}{Re} [\frac{\partial^2 U}{\partial X^2} + \frac{\partial^2 U}{\partial Y^2}], \\ \frac{\partial p}{\partial Y} &= [-\ddot{\alpha}(t)X + \dot{\alpha}^2(t)Y - \ddot{h}(t) \cos(\alpha(t))] + \frac{1}{Re} [\frac{\partial^2 V}{\partial X^2} + \frac{\partial^2 V}{\partial Y^2}]. \end{cases}$$

Derivatives of the velocity components can be expressed in terms of the stream function as:

$$\begin{cases} \frac{\partial U}{\partial X} = -\frac{\partial V}{\partial Y} = \frac{1}{j^2} \left[\cos 2\theta \frac{\partial X}{\partial \xi} \frac{\partial Y}{\partial \zeta} + \frac{\sin 2\theta}{2} \left(\frac{\partial Y}{\partial \zeta} \frac{\partial X}{\partial \xi} + \frac{\partial Y}{\partial \xi} \frac{\partial X}{\partial \zeta} \right) \right] \frac{\partial^2 \psi}{\partial r^2}, \\ \frac{\partial U}{\partial Y} + \frac{\partial V}{\partial X} = \frac{1}{j^2} \left[\cos 2\theta \left(\left(\frac{\partial X}{\partial \zeta} \right)^2 - \left(\frac{\partial X}{\partial \xi} \right)^2 \right) - 2 \sin 2\theta \frac{\partial X}{\partial \zeta} \frac{\partial X}{\partial \xi} \right] \frac{\partial^2 \psi}{\partial r^2}, \end{cases}$$

whereas the Laplacian of U and V are written in terms of the vorticity as:

$$\begin{cases} \Delta U = \frac{1}{j} \frac{\partial X}{\partial \zeta} \left[\cos \theta \frac{\partial \omega}{\partial r} - \frac{\sin \theta}{r} \frac{\partial \omega}{\partial \theta} \right] - \frac{1}{j} \frac{\partial X}{\partial \xi} \left[\sin \theta \frac{\partial \omega}{\partial r} + \frac{\cos \theta}{r} \frac{\partial \omega}{\partial \theta} \right], \\ \Delta V = \frac{1}{j} \frac{\partial Y}{\partial \zeta} \left[\cos \theta \frac{\partial \omega}{\partial r} - \frac{\sin \theta}{r} \frac{\partial \omega}{\partial \theta} \right] - \frac{1}{j} \frac{\partial Y}{\partial \xi} \left[\sin \theta \frac{\partial \omega}{\partial r} + \frac{\cos \theta}{r} \frac{\partial \omega}{\partial \theta} \right]. \end{cases}$$

Appendix B. The gradient relations

The derivatives included in the gradient are computed through the following relations:

$$\begin{cases} \frac{\partial F_x}{\partial \omega} \frac{d\omega}{dg} = -\int_0^{2\pi} \left(\frac{\partial p}{\partial \omega} \frac{d\omega}{dg} \right) \frac{\partial Y}{\partial \theta} d\theta, & \frac{\partial F_x}{\partial g} = -\int_0^{2\pi} \left(\frac{\partial p}{\partial g} \right) \frac{\partial Y}{\partial \theta} d\theta \\ \frac{\partial F_y}{\partial \omega} \frac{d\omega}{dg} = \int_0^{2\pi} \left(\frac{\partial p}{\partial \omega} \frac{d\omega}{dg} \right) \frac{\partial X}{\partial \theta} d\theta, & \frac{\partial F_y}{\partial g} = \int_0^{2\pi} \left(\frac{\partial p}{\partial g} \right) \frac{\partial X}{\partial \theta} d\theta \\ \frac{\partial M_z}{\partial \omega} \frac{d\omega}{dg} = \int_0^{2\pi} \left(\frac{\partial p}{\partial \omega} \frac{d\omega}{dg} \right) (X \frac{\partial X}{\partial \theta} + Y \frac{\partial Y}{\partial \theta}) d\theta, & \frac{\partial M_z}{\partial g} = \int_0^{2\pi} \left(\frac{\partial p}{\partial g} \right) (X \frac{\partial X}{\partial \theta} + Y \frac{\partial Y}{\partial \theta}) d\theta \\ \frac{\partial p}{\partial \omega} \frac{d\omega}{dg} = \int_0^{2\pi} \frac{\partial X}{\partial \theta} \frac{1}{Rej} \left[\left(-\frac{\partial X}{\partial \zeta} \cos \theta + \frac{\partial X}{\partial \xi} \sin \theta \right) \frac{\partial \omega_g}{\partial r} + \frac{1}{r} \left[\frac{\partial X}{\partial \zeta} \sin \theta + \frac{\partial X}{\partial \xi} \cos \theta \right] \frac{\partial \omega_g}{\partial \theta} \right] d\theta \\ \quad + \int_0^{2\pi} \frac{\partial Y}{\partial \theta} \frac{1}{Rej} \left[\left(\frac{\partial Y}{\partial \zeta} \cos \theta - \frac{\partial Y}{\partial \xi} \sin \theta \right) \frac{\partial \omega_g}{\partial r} - \frac{1}{r} \left[\frac{\partial Y}{\partial \zeta} \sin \theta + \frac{\partial Y}{\partial \xi} \cos \theta \right] \frac{\partial \omega_g}{\partial \theta} \right] d\theta \\ \frac{\partial p}{\partial g} = \int_0^{2\pi} \frac{\partial}{\partial g} \left(\dot{\alpha}(t)Y + \dot{\alpha}^2(t)X - \ddot{h}(t) \sin(\alpha(t)) \right) \frac{\partial X}{\partial \theta} d\theta \\ \quad + \int_0^{2\pi} \frac{\partial}{\partial g} \left(-\ddot{\alpha}(t)X + \dot{\alpha}^2(t)Y - \dot{h}(t) \cos(\alpha(t)) \right) \frac{\partial Y}{\partial \theta} d\theta \end{cases}$$

and

$$\begin{cases} \frac{\partial F_x}{\partial \psi} \frac{d\psi}{dg} = \frac{1}{Re} \int_0^{2\pi} \frac{2}{j^2} \frac{\partial Y}{\partial \theta} \left[\cos 2\theta \frac{\partial X}{\partial \zeta} \frac{\partial Y}{\partial \xi} + \frac{\sin 2\theta}{2} \left(\frac{\partial Y}{\partial \zeta} \frac{\partial X}{\partial \xi} + \frac{\partial Y}{\partial \xi} \frac{\partial X}{\partial \zeta} \right) \right] \frac{\partial^2 \psi_g}{\partial r^2} d\theta \\ \quad - \frac{1}{Re} \int_0^{2\pi} \frac{1}{j^2} \frac{\partial X}{\partial \theta} \left[\cos 2\theta \left(\left(\frac{\partial X}{\partial \zeta} \right)^2 - \left(\frac{\partial X}{\partial \xi} \right)^2 \right) - 2 \sin 2\theta \frac{\partial X}{\partial \zeta} \frac{\partial X}{\partial \xi} \right] \frac{\partial^2 \psi_g}{\partial r^2} d\theta \\ \frac{\partial F_y}{\partial \psi} \frac{d\psi}{dg} = \frac{1}{Re} \int_0^{2\pi} \frac{2}{j^2} \frac{\partial X}{\partial \theta} \left[\cos 2\theta \frac{\partial X}{\partial \zeta} \frac{\partial Y}{\partial \xi} + \frac{\sin 2\theta}{2} \left(\frac{\partial Y}{\partial \zeta} \frac{\partial X}{\partial \xi} + \frac{\partial Y}{\partial \xi} \frac{\partial X}{\partial \zeta} \right) \right] \frac{\partial^2 \psi_g}{\partial r^2} d\theta \\ \quad + \frac{1}{Re} \int_0^{2\pi} \frac{1}{j^2} \frac{\partial Y}{\partial \theta} \left[\cos 2\theta \left(\left(\frac{\partial X}{\partial \zeta} \right)^2 - \left(\frac{\partial X}{\partial \xi} \right)^2 \right) - 2 \sin 2\theta \frac{\partial X}{\partial \zeta} \frac{\partial X}{\partial \xi} \right] \frac{\partial^2 \psi_g}{\partial r^2} d\theta \\ \frac{\partial M_z}{\partial \psi} \frac{d\psi}{dg} = \int_0^{2\pi} \left(\frac{2}{Rej^2} \right) (X \frac{\partial X}{\partial \theta} - Y \frac{\partial Y}{\partial \theta}) \left[\cos 2\theta \frac{\partial X}{\partial \zeta} \frac{\partial Y}{\partial \xi} + \frac{\sin 2\theta}{2} \left(\frac{\partial Y}{\partial \zeta} \frac{\partial X}{\partial \xi} + \frac{\partial Y}{\partial \xi} \frac{\partial X}{\partial \zeta} \right) \right] \frac{\partial^2 \psi_g}{\partial r^2} d\theta \\ \quad + \int_0^{2\pi} \frac{1}{Re} \left(X \frac{\partial Y}{\partial \theta} + Y \frac{\partial X}{\partial \theta} \right) \frac{1}{j^2} \left[\cos 2\theta \left(\left(\frac{\partial X}{\partial \zeta} \right)^2 - \left(\frac{\partial X}{\partial \xi} \right)^2 \right) - 2 \sin 2\theta \frac{\partial X}{\partial \zeta} \frac{\partial X}{\partial \xi} \right] \frac{\partial^2 \psi_g}{\partial r^2} d\theta \end{cases}$$

References

- [1] Anderson JM. Vortex control for efficient propulsion. PhD Thesis, Joint Program, MIT & Woods Hole Oceanographic Ins.; 1996
- [2] Anderson JM, Streitlien K, Barret DS, Triantafyllou MS. Oscillating foils for high propulsive efficiency. *J Fluid Mech* 1998;360:41–72.
- [3] Bejan A, Marden JH. Unifying constructal theory for scale effects in running, swimming and flying. *J Exp Biol* 2005;209:238–48.
- [4] Bozkurtas M, Dong H, Seshadri V, Mittal R, Najjar F. Towards numerical simulation of flapping foils on fixed Cartesian grids. *AIAA Paper* 2005;2005-79.
- [5] Braza M, Chassaing P, Minh HH. Numerical study and physical analysis of the pressure and velocity fields in the near wake of a circular cylinder. *J Fluid Mech* 1986;165:79–130.
- [6] Canan JW. Seeing more and risking less with UAVs. *Aerospace Am* 1999:26–31.
- [7] Guermont JL, Quartapelle L. Uncoupled $\omega - \psi$ formulation for plane flows in multiply connected domains. *Math Models Methods Appl Sci* 1997;7(6):731–67.
- [8] Grasmeyer JM, Keennon MT. Development of the Black Widow micro air vehicle. In: Muller TJ, editor. Fixed and flapping wing aerodynamics for micro air vehicle applications. Progress in astronautics and aeronautics. Reston, VA: AIAA; 2001. p. 519–35.
- [9] Guerrero J. Efficient treatment of complex geometries and moving bodies using overlapping grids. In: 10th ISGG conference on numerical grid generation, September 16–20, 2007, FORTH, Crete, Greece.
- [10] Guglielmi L. Modeling of thrust generating foils. PhD Thesis, University of Genoa; 2004.
- [11] Guglielmi L, Blondeaux P. Propulsive efficiency of oscillating foils. *Eur J Mech B Fluids* 2004;23(2):255–78.
- [12] Gunzburger MD. Inverse design and optimization methods: introduction into mathematical aspects of flow control and optimization. von Karman Institute for Fluid Dynamics Lecture Series 1997, 1997-05.
- [13] Hewish M. Building a bird's-eye view for the battlefield. *Jane Int Defense Rev* 1997;55–61.
- [14] Isogai K, Shinmoto Y, Watanabe Y. Effects of dynamic stall on propulsive efficiency and thrust of flapping foil. *AIAA J* 1999;37(10):1145–51.
- [15] Kroo I, Kunz P. Mesoscale flight and miniature rotorcraft development. In: Muller TJ, editor. Fixed and flapping wing aerodynamics for micro air vehicle applications. Progress in astronautics and aeronautics. Reston, VA: AIAA; 2001. p. 503–17.
- [16] Lewin GC, Haj-Hariri H. Modelling thrust generation of a two-dimensional heaving airfoil in a viscous flow. *J Fluid Mech* 2003;492:339–62.
- [17] Lighthill MJ. Note on the swimming of slender fish. *J Fluid Mech* 1960;9:305–17.
- [18] McMasters JH, Henderson ML. Low speed single element airfoil synthesis. *Tech Soaring* 1980;2(2):1–21.
- [19] Ohmi K, Coutanceau M, Loc TP, Dulieu A. Vortex formation around an oscillating and translating airfoil at large incidences. *J Fluid Mech* 1990;311:37–60.
- [20] Pedro GH, Suleman A, Djilali N. A numerical study of the propulsive efficiency of a flapping hydrofoil. *Int J Numer Methods Fluids* 2003;42(5):493–526.
- [21] Ramamurti R, Sandberg W. Computational study of 3-D flapping foils. *AIAA Paper* 2001;2001-0605.
- [22] Rayner JMV. Form and function in avian flight. *Curr Ornithol* 1988;5:1–77.
- [23] Read DA, Hover FS, Triantafyllou MS. Forces on oscillating foils for propulsion and maneuvering. *J Fluids Struct* 2003;17:163–83.
- [24] Silin D, Malladi B, Shkarayev S. The University of Arizona micro Ornithopters. The 2nd US-European Competition and Workshop on Micro Air Vehicles, Sandestin, FL, October 30–November 2, 2006.
- [25] Smith RW, Wright JA. Simulation of the propulsion characteristics of a flapping AUV. *AIAA Paper* 2005;2005-4758.
- [26] Spedding GR, DeLaurier JD. Animal and ornithopter flight. In: Schetz JA, Fuhs AE, editors. Handbook of fluid dynamics and fluid machinery. Applications of fluid dynamics, vol. 3. New York: Wiley; 1996. p. 1951–67.
- [27] Streitlien K, Triantafyllou GS, Triantafyllou MS. Efficient foil propulsion through vortex control. *AIAA J* 1996;34:2315–9.
- [28] Taylor GK, Nudds RL, Adrian LRT. Flying and swimming animals cruise at a Strouhal number tuned for high power efficiency. *Nature* 2003;425:707–11.
- [29] Triantafyllou GS, Triantafyllou MS, Grosenbaugh MA. Optimal thrust development in oscillating foils with application to fish propulsion. *J Fluids Struct* 1993;7:205–24.
- [30] Tuncer IH, Kaya M. Optimization of flapping airfoils for maximum thrust and propulsive efficiency. *AIAA J* 2005;43(11):2329–36.
- [31] Wang ZJ. Vortex shedding and frequency selection in flapping flight. *J Fluid Mech* 2000;410:323–41.